PCCP

Accepted Manuscript

PCCP RSCPublishing

PAPER

Optical and magnetic properties of $Ba_5(BO_3)_3F$ single crystals

Cite this: DOI: 10.1039/x0xx00000x

Received 00th January 2012,
Accepted 00th January 2012

DOI: 10.1039/x0xx00000x

www.rsc.org/

A.P. Yelisseyev[*,1], Xingxing Jiang[2,3] V.P. Solntsev[1], T.B.Bekker[1], Zheshuai Lin[*,2]

$Ba_5(BO_3)_3F$ single crystals of high optical quality and up to 1.5 cm in section were grown. Its transparency range is 0.23 to 6.6 μm (on 10% level). Direct allowed electronic transitions at Γ-point give band gap values are 5.31 and 5.40 eV at 300 and 80 K, respectively. Luminescence is excited in the near-edge absorption bands near 265 and 365 nm. X-irradiation induces additional absorption in dominating 252, 317 and 710 nm bands. Combined electron spin-resonance spectroscopy and theoretical analysis allow one to associate three absorption peaks with O^{5-}, O^{1-} and e_6^- (fluorine vacancy), respectively. Original transparency restores after crystal heating to 400 K and charge carriers release from traps with E_T=0.87 eV, s=10^{12} sec^{-1}. Dispersion curves for refractive indices were calculated and Sellmeier equations were built. Theoretical analysis shows strong localization of the Ba 5s and F 2s orbitals, strong ionicity of Ba cations and strong covalency of B-O bond. Optical properties of $Ba_5(BO_3)_3F$ are dominantly determined by the electron transition within $(BO_3)^{3-}$ groups, despite the transition between barium and oxygen also have a little contribution.

Introduction

Recent studies of the BaF_2-$Ba_3(BO_3)_2$ system led to the discovery of two new intermediate fluoroborate phases: $Ba_7(BO_3)_{4-y}F_{2+3y}$ and $Ba_5(BO_3)_3F$ [1-3]. The former represents a solid solution series where the area of homogeneity spans between $Ba_7(BO_3)_{3.79}F_{2.63}$ and $Ba_7(BO_3)_{3.35}F_{3.95}$ compositions (0.21<y<0.65) as a result of $(BO_3)^{3-} \leftrightarrow 3F^-$ anionic substitution. In contrast, no evidence of substitution was found in the $Ba_5(BO_3)_3F$ phase.

The structure of $Ba_5(BO_3)_3F$ is centrosymmetric and cannot be used in nonlinear optics. Nevertheless this wide band-gap material can be utilized for different optical devices such as Glan polarizers etc. Unfortunately, to date there is no information about the optical properties of this crystal. In present work single crystals of $Ba_5(BO_3)_3F$ of optical quality were grown and their optical properties and point defects were investigated using optical luminescence/absorption spectroscopy, and electron spin-resonance (ESR) spectroscopy. Meanwhile, the electronic and optical properties including the band structure, total and partial densities of states, refractive indices dispersion and birefringence in $Ba_5(BO_3)_3F$ were determined by the first-principles theory, and the absorption due to anion vacancies was studied.

Results and discussion

Crystal structure

The unfaceted round boule up to 1.5 cm in section was obtained and the appearance and PL pattern of the polished plate are shown in Fig.1. According to X-ray structural analysis $Ba_5(BO_3)_3F$ crystallizes in rhombic syngony, *Pnma*, with the lattice parameters of a=7.60788(12) Å, b=14.8299(2) Å, c=10.28650(16) Å. The crystal density is 5.049 g/cm[33].

The structural study reveals that $Ba_5(BO_3)_3F$ is isostructural to the $Sr_5(BO_3)_3F$ phase described by Alekel & Keszler[4] . We believe that the most convenient and best fitting depiction of such structures is by the model made up of a cation sublattice with anion-filled cavities, similar to the model suggested for alkali-earth borates by Vegas[5]. The $Ba_5(BO_3)_3F$ lattice has the following three types of cation-coordinated anions (shown in Fig.2): (1) F^- situated in octahedral face linked into columns and $(BO_3)^{3-}$ triangles occupying either (2) three-capped trigonal prisms or (3) distorted tetragonal antiprisms. As no evidence of anionic substitution in $Ba_5(BO_3)_3F$ has been obtained, it is most likely that the $(BO_3)^{3-}$ anions with such coordination are incapable of producing $(BO_3)^{3-} \leftrightarrow 3F^-$ isomorphism.

Transmission/absorption and luminescence

Fig.3 displays the transmission spectra for polished $Ba_5(BO_3)_3F$ plates 2 and 0.5 mm thick at 80 and 300 K. At 300 K samples are transparent in a wide spectral range from 234 nm to 6.6 μm in the mid –IR (on the 10% level, at 300 K). As temperature decreases to 80 K, the edge shifts to 229 nm. One can see absorption bands near 265 nm and 365 nm with Full width at half-maximum (FWHM) values of about 0.8 and 0.4 eV, respectively (Fig.3a). They are pronounced better in a thicker plate. There is some fine structures in the 3 to 6 μm range. Transparency edge at long wavelengths is known to depend on mass of the ions in the compound. It is expected that the presence of heavy Ba as well as a partial fluorine substitution for oxygen results in the red-shift of IR absorption edge in $Ba_5(BO_3)_3F$ to longer wavelengths. Compared with the famous optical crystals β-BaB_2O_4 (BBO), LiB_3O_5 (LBO) and $CsLiB_6O_{10}$ (CLBO), in which the IR edges occur at 1.8 μm and crystals become opaque near 3.5 μm, $Ba_5(BO_3)_3F$ begins to absorb near 2.8 μm whereas complete absorption occurs near 6.7 μm. Windows with residual transparency up to 60 % are observed in $Ba_5(BO_3)_3F$ near 4.3, 5.3, 5.8 and 6.2 μm.

Analysis of the shape of absorption spectrum for a thin $Ba_5(BO_3)_3F$ plate showed that the spectrum can be approximated by a straight line when represented in coordinates $(\alpha\times h\nu)^2$ and $(h\nu)$ (insert in Fig.3a). Here α is absorption coefficient and $h\nu$ is photon energy. It means that direct allowed electronic transitions are responsible for the fundamental absorption edge[13]. The points of intersection between straight line and the abscissa axis reveal that the band gap values are 5.420 and 5.305 eV at 80 and 300 K, respectively.

X-ray irradiation produces some additional absorption in $Ba_5(BO_3)_3F$. Absorption spectra recorded for $Ba_5(BO_3)_3F$ at 300 K, before and after X-ray irradiation, as well as a differential spectrum are given in Fig.4. Differential spectrum is shown with ×4 magnification for clarity. After X-ray irradiation the absorption at $\lambda <$ 900 nm increases and a set of bands with maximums near 252, 317, 532 and 710 nm are well-pronounced. These new bands at short waves do not consist with the already existing absorption bands. Thus, X-irradiation changes the charge state of several types of centers and new absorption bands correspond to these new charge states. Charge carriers released at X-irradiation are partly localized in the capture centers. Generally the relaxation to original equilibrium state takes place as time goes by. The rate of this relaxation is determined by the parameters of these capture centers and it can be increased by a long wavelength illumination or by sample heating. Since crystals contain heavy Ba ions and have large density (5.049 g/cm^3) X-rays penetrate only a thin near-surface layer of about 50 μm thick and only in this layer the new absorption appears.

Kinetics of crystal coloring at X-irradiation, recorded for 500 nm wavelength, is given in the inset in Fig. 4. Here point 1 shows absorption before irradiation (close to 0) and points 1 to 5 all together demonstrate kinetics for irradiation through one face of polished $Ba_5(BO_3)_3F$ plate. one can see a fast saturation (during ~1 hour). If we turn the plate over and irradiate it further through the opposite face, absorption continues to increase again. Afterwards sample becomes slightly yellow. This means that the X-ray bombardment dominantly affects the near-surface layers by making them colored, whereas the main bulk remains uncolored.

It should be emphasized that the X-ray induced absorption is relatively instable in $Ba_5(BO_3)_3F$: the color disappears spontaneously for a day of storage at room temperature in the darkness and this process becomes much faster if sample is exposed to the visible light with $360<\lambda<630$ nm. This phenomenon actually suggests that the optical absorption should be resulted from the electron in the capture center. Electron becomes free and may diffuse to an ionized center with its further return to initial charge state. Moreover, such release of an electron and the subsequent radiative relaxation can take place when sample is heated. The fact that the X-ray induced absorption can be removed by a long wave illumination implies that the X-ray irradiation does not produce new defects in the $Ba_5(BO_3)_3F$ lattice but mainly changes the charge state of already existing defects.

A curve of thermoluminescence (TL) recorded after X-irradiation at 80 K is given in Fig. 5. There is only one TL peak centered near 314 K with FWHM=32 K. Since TL peak is located very close to room temperature the electrons can easily release from the corresponding capture centers. This agrees well the fact of fast $Ba_5(BO_3)_3F$ relaxation in the darkness at room temperature.

The shape of the TL peak is described rather well by the following equation[14] :

$$I(t) = n_0 s \cdot \exp(-E_T / kT) \cdot \exp\left[-(s/\beta) \int_{T_0}^{T} \exp(-E_T / k\theta) d\theta \right] \quad (1)$$

where n_0 is the initial concentration of electrons captured by the traps, s is the effective frequency factor, β is the rate of linear heating, k is Boltzmann's constant, E_T is the energy of thermal activation (eV) and T_0 is the initial temperature. Thus, one can obtain that the energy of thermal activation for this center is E_T=0.87 eV with the effective frequency factor of $s=10^{12}$ sec^{-1}.

Photoluminescence(PL) spectra for $Ba_5(BO_3)_3F$ are given in Fig.6. At 325 nm excitation one observed a dominating 398 nm band with a satellite near 351 nm as well as two other bands at 520 and 720 nm (curve 1). Excitation near 365 nm produced white PL in a broad 520 nm band (curve 2). At 532 nm excitation there was a broad band near 630 nm (curve 3). One can suppose that PL bands near 398 and 520 nm are due to radiative relaxation in the defects responsible for 265 and 365 nm absorption bands (Fig.3a), while there should be also a weaker absorption band near 530 nm. Corresponding center is responsible for the 630 nm PL emission. PL is associated mainly with internal radiative transitions. X-ray irradiation produces X-ray excited luminescence (RL) emission in a broad 398 nm band (curve 4), which is very similar to that in PL at 325 nm excitation. However, the RL band is almost twice broader in comparison with PL: FWHM values for them are 0.75 and 0.4 eV, respectively. Broadband RL is supposed to be excited in a thin near-surface layer of $Ba_5(BO_3)_3F$, several tens μm thick, with point defects distorted after mechanical treatment.

ESR

ESR is a well-known powerful technique used to determine the structure of point defects in solids. No signal was observed in ESR spectra of as-grown fluoroborates $Ba_5(BO_3)_3F$. However, after X-ray irradiation signals from both electron-type and hole-type centers appeared (Fig.7). The electron-type center is an electron captured on a fluorine vacancy located in the Ba_6 octahedron. Analysis of the angular dependence for the ESR lines showed that electron-type e_6^- center has g-factor $g_c=1.966\pm0.001<g_e=2.0023$ (the value for free electron) and there are two magnetically nonequivalent complexes in the crystal structure. The center structure coincides well with an expected fluorine position in the $Ba_5(BO_3)_3F$ lattice. Such defects are well-known as F-centers in literature[15]. One can see also signals from two hole-type (O_1^- and O_5^-) in Fig.7. They are oxygen ions which have captured a hole (or lost an electron). Center O_1^- is due to a hole on oxygen O_1^- (R_{O1-F}= 3.081Å) interacting with one ^{19}F atom. Parameters of this center at H‖c are g_c = 2.0118 and A_c = 11 G. In the other hole-like center a hole on other oxygen interacts with one ^{19}F atom (R_{O5-F}= 3.159Å) and the parameters are g_c= 2.0048, A_c = 3.5 G. ESR spectra of these paramagnetic centers are described well by the spin-Hamiltonian[16]:

$$H = \beta \hat{g} \hat{S} \hat{H} + \hat{A} \hat{S} \hat{I}, \quad \hat{S} = ½, \quad \hat{I} = ½ . \quad (2)$$

where $\hat{A}$ is a constant of hyperfine interaction between an unpaired electron and the fluorine atom ^{19}F with nuclear magnetic moment $\hat{I}$ = ½ and natural abundance of 100%. According to structural data[2] $Ba_5(BO_3)_3F$ is characterized by a rhombic symmetry (space group Pnma). Atoms Ba_1, B_2, F, O_4, O_5, O_6 occupy the “4c” positions with C_s symmetry in the structure, whereas atoms Ba_2, Ba_3, B_1, O_1, O_2, O_3 occupy the“8d” sites (C_1). One should note that fluorine atoms F^- are surrounded by six Ba^{2+} cations and by six O^{2-}. Distances Ba –F vary from 2.621 to 3.452 Å, while O_1 –F = 3.081 and 3.476 Å, O_5 –F = 3.159, O_6-F = 3.250 Å. The hole centers O_1 and O_5 are a result of hole capture by the oxygens which are closer to F^-. Paramagnetic centers in the “4c”position have two magnetically nonequivalent positions and one axis of g-tensor which coincides with [010] of the crystal. Centers in the “8d” position have four magnetically nonequivalent positions in the structure.

Principal values of g-tensors for these centers are the following: for O_1^- g_z = 2.0088, g_y = 2.0803, g_x = 2.1074; for O_5^- – g_z = 2.0048, g_y = 2.0791, g_x = 2.0828. It was established that principal axes of g and A tensors do not coincide for these centers. The most appropriate explanation for positive g_z deviation from g_e = 2.0023, which is maximal for O_1^-, is a transfer of spin density of defect electron from O_1^- $2p_z$ orbital to the equatorial O^{2-} ions. To date we couldn’t record the angular dependence for ESR lines completely. However, obtained data are enough to analyze the splitting of p –levels for O_1^- and O_5^- ions. Crystalline field splits p state so, that p_z becomes the lower state.

As showed O’Brian[17] for principal values of g-tensor the following ratios should be valid:

$$g_\perp = (g_x + g_y)/2, \quad g_x = g_e + 2\lambda\varepsilon^2/E_x, \quad g_y = g_e + 2\lambda\varepsilon^2/E_y, \quad (3)$$

where g_e = 2.0023 is g –factor value for a free electron, λ is the constant of spin-orbital bonding, ε^2 is a coefficient which takes into account a degree of covalent bonding and $E = (E_x + E_y)/2$. Using the value λ_O^- = -150 cm^{-1} and ε^2 = 0.86[18] we obtain for O_1^- : $E_x \approx$ 2500 cm^{-1}, $E_y \approx$ 3300 cm^{-1} and E ≈ 2820 cm^{-1}. For O_5^- we have: $E_x \approx$ 3200 cm^{-1}, $E_y \approx$ 3400 cm^{-1}. Here E_x, E_y are distances between p_z level and the p_x, p_y levels of the O^- ion in the ground state, respectively. Thus, all these transitions fall into mid-IR spectral range (2.9-3.1 μm) and it is difficult to separate them from the native vibrations of $Ba_5(BO_3)_3F$ structural fragments (Fig.3b). Third order of perturbation theory predicts the following $g_\parallel$ deviation from the free electron value g_e = 2.0023: $\Delta g_\parallel = -\lambda^2/E_1^2 \cdot (g_e-1) = -\{\Delta g_\perp^2/2\}^2 \cdot (g_e-1)$ or $E_1 = (2\lambda\varepsilon^2/\Delta g_\perp^2)$. Here E_1 is a distance between ground and first excited states of the O- ion. Taking experimentally measured values of $\Delta g_\perp$ we may estimate E_1. Thus, for O_1^- we have $E_1 \approx$ 30800 cm^{-1} which corresponds to 325 nm in the wavelength scale. In the same way for O_5^- we obtain $E_1 \approx$ 42400 cm^{-1} (235 nm). Thus two broad bands near 252 and 317 nm in absorption spectra of X-irradiated $Ba_5(BO_3)_3F$ samples may be related to paramagnetic O_5^- and O_1^- centers, respectively. Fast color saturation at X-ray irradiation allows one to suppose that not every regular oxygen ion may be ionized but only some of them, supposedly those near some defects (maybe impurity ones). The remaining two bands near 532 and 705 nm in Fig,4 may be related to other point defects such as F-center (e_6^-).

Electronic and optical properties by computer simulations

Figure 8a displays the electron band structure near the forbidden band of $Ba_5(BO_3)_3F$ along the lines of high symmetry point. It is clearly shown that $Ba_5(BO_3)_3F$ is a typical direct band gap insulator, with both maximum of valence band (VB) and minimum of conduction band (CB) located at gamma point. This is in accordance with the experimental results of fundamental absorption analysis (Fig.3a). The calculated energy band gap is E_g = 3.66 eV, which is smaller than the measured value of 5.31 eV. Such underestimation for E_g is typical when one uses the GGA method[19,20]. In Fig.8b position of the level of F-center (fluorine vacancy) is shown. One can see that it is located approximately 1.8 eV above the VB maximum.

Figure 9a shows the total density of state (TDOS) and partial density of state (PDOS) projected in the constitute atoms. The following electronic characteristics can be deduced: (i) The Ba 5s and F 2s orbitals are strongly localized at the deep energy level (around -25 eV and -20 eV) and have very little hybridization with other orbitals. These orbitals are difficult to be simulated by exterior perturbation and contribute little to the optical properties related to the electron transitions inside the forbidden band; (ii) The electron energy between -20 eV and -10 eV is mainly composed of Ba 5p, O 2s and B 2p orbitals. The sharp peaks occurring at about -9 eV reveal the strong ionicity of barium cations; and (iii) The top of VB mainly constitute of B 2p, O 2p and F 2p orbitals, and the bottom of CB is composed of B 2p, O 2p and Ba 5d orbitals. The hybridization between B 2p and O 2p orbitals in the wide energy range indicates the strong covalency of B-O bond. Moreover, since both B and O orbitals are located at the top of VB and the bottom of CB, the optical properties of $Ba_5(BO_3)_3F$ are dominantly determined by the electron transition within $(BO_3)^{3-}$ groups, despite the transition between barium and oxygen also have a little contribution.

The crystal symmetry of $Ba_5(BO_3)_3F$ belongs to Pnma space group and biaxial crystal system. Figure 10 exhibits the calculated dispersion curves of refractive indices n_x, n_y, n_z. The birefringence value is about 0.02 at the wavelength of 1064 nm. Although the $(BO_3)^{3-}$ group has relatively large microscopic optical anisotropy[21], the disoriented arrangement of these groups results in the relatively small birefringence in $Ba_5(BO_3)_3F$. According to the dispersion curve, Sellmeier equations constructed for $Ba_5(BO_3)_3F$ are given below:

$$n_x^2 = 2.7771 + \frac{0.0226}{\lambda^2 - 0.0228} - 0.0009\lambda^2 \quad (4a)$$

$$n_y^2 = 2.8166 + \frac{0.0230}{\lambda^2 - 0.0208} - 0.0006\lambda^2 \quad (4b)$$

$$n_z^2 = 2.8548 + \frac{0.0239}{\lambda^2 - 0.0218} - 0.0008\lambda^2 \quad (4c)$$

One of the prevalent point defects in $Ba_5(BO_3)_3F$ is the anion vacancy e_6^- . Figure 11 shows the charge density difference contour maps around the fluorine vacancy. By removing a neutral fluorine atom from unit cell, one electron is left in the lattice unboundedly, so forming the e_6^- vacancy. One can see that the charge density redistribution around the e_6^- defect is quite localized. The optical absorption spectrum of the $Ba_5(BO_3)_3F$ with defect e_6^- is shown in Fig. 12. Meanwhile, the absorption spectrum of perfect $Ba_5(BO_3)_3F$ is also shown for comparison. It is clearly shown that the absorption spectrum of perfect $Ba_5(BO_3)_3F$ are in good agreement with the measured one, validating the feasibility of plane-wave method to the calculation of optical properties of $Ba_5(BO_3)_3F$. For the defect e_6^- a strong absorption peak centered near 2.0 eV (620 nm) occurs in the calculated absorption spectrum. This spectrum is similar to that for $Ba_5(BO_3)_3F$ after X-irradiation (Fig.4) although the latter is located near 1.74 eV (710 nm). One can see that after X-irradiation both calculated (Fig.12) and experimental (Fig. 4) absorption spectra in the visible region/near IR region are non-elementary: in both cases dominating band has a shoulder at short waves related supposedly to the same defect. Thus we suppose that a strong band near 710 nm is associated with paramagnetic fluorine vacancy.

Conclusions

In this work, the $Ba_5(BO_3)_3F$ single crystals of optical quality, up to 1.5 cm in section were obtained. Consequently, the absorption, luminescence and ESR spectra were measured and the first-principles studies on electronic and optical properties were performed. Some useful conclusions are summarized as follows:

(1) Transparency range in $Ba_5(BO_3)_3F$ single crystal is 0.23 to 6.6 μm (on 10% transmission level) and band gap values are 5.31 and 5.40 eV at 300 and 80 K, respectively. Analysis of fundamental absorption shape and *ab initio* calculations indicate these E_g values to be a result of direct allowed electronic transitions at Gamma point. Two absorption bands near 265 and 365 nm are observed at short wavelengths.

(2) X-irradiation results in additional absorption in dominating 252, 317 and 710 nm bands. Combined ESR and theoretical analysis allowed one to associate them with O_5^-, O_1^- and e_6^- (fluorine vacancy), respectively. Some charge carriers are captured at traps with E_T=0.87 eV, $s=10^{12}$ sec^{-1}: they are released at heating to 350 K and original transparency restores.

(3) Refractive indices vary in the 1.68 to 1.78 range at 0.3 to 3 μm. Dispersion curves for refractive indices were calculated and Sellmeier equations were built. The birefringence is about 0.02, and the relatively weak optical anisotropy is mainly due to the disoriented arrangement of the $(BO_3)^{3-}$ groups.

(4) Analysis of TDOS and PDOS patterns shows strong localization of the Ba 5s and F 2s orbitals and strong ionicity of barium cations and strong covalency of B-O bond. Optical properties of $Ba_5(BO_3)_3F$ are dominantly determined by the electron transition within $(BO_3)^{3-}$ groups, despite the transition between barium and oxygen also have a little contribution.

Experimental and computational details

Crystal growth

$Ba_5(BO_3)_3F$ melts incongruently at 1175 ºC[3]. For crystal growth we chose the composition 30 mol. % BaB_2O_4, 15 mol. % BaF_2, 55 mol. % BaO in BaB_2O_4 – BaF_2 – BaO ternary system as studied in Ref. [1] in detail. Commercially available $BaCO_3$, H_3BO_3 and BaF_2 of high purity grade were used as starting reagents. The experiment on crystal growth was carried out in a furnace with precise (±0.1 ºC) temperature control (Eurotherm 2604). The single crystals were grown on a platinum loop in air. The solution (30 g) was melted in a platinum crucible (40 mm in diameter) through the solid-stage synthesis. Heating rate was 25 ºC/hour; the maximum heating temperature was 1100 ºC. At this temperature the melt was kept with periodic mechanical stirring for 24 hours for homogenization. The liquidus temperature of about 1000 ºC was determined by visual polythermal analysis. At this temperature a platinum loop was placed into the central part of the melt surface to induce the spontaneous crystallization. From the moment of detection of spontaneous microcrystals, the solution was cooled at a rate of 0.5 °C/day for 7 days in order to increase crystals size. Then the platinum loop with grown crystals was extracted from the melt and cooled to room temperature at a rate 15 °C/hour. These allow us to grow crystals up to $15 \times 12 \times 3$ mm^3 in size.

Optical spectroscopy

Transmission spectra were recorded with a UV-2501PC Shimadzu spectrometer in the UV – to-near IR, whereas in the mid-IR we used a Fourier-Transform spectrometer Infralum 801. The photoluminescence (PL) spectra were measured using a SDL1 diffraction luminescence spectrometer with excitation from a 1 kW Xe lamp through MDR2 diffraction monochromator. X-ray excited luminescence (RL) was recorded with a MDR2 diffraction monochromator with a FEU100 photomultipliers as emission detector. A table 1 kW X-ray set-up with a W-anticathode tube, at 40 KV voltage and 20 mA current was used in experiments on RL and X-ray induced absorption. PL and Raman spectra were recorded using a LabRAM spectrometer from Horiba, at 325 nm and 514 nm laser excitation, at T=300 K. Thermoluminescence curves were recorded when heating sample at β=0.33 K/sec rate after preliminary low temperature (at 80 K) photo- or X-ray excitation.

ESR

The ESR spectra of $Ba_5(BO_3)_3F$ samples were recorded at frequency 9.3 GHz and temperatures 300 and 77 K with a spectrometer RE 1306 designed at the institute of chemical kinetics and combustion SB RAS (Novosibirsk, Russia).

Computational method

The first-principles calculations on $Ba_5(BO_3)_3F$ were performed by CASTEP[6], a plane-wave pseudopotential total-energy package based on density functional theory (DFT)[7] . The functionals developed by Perdew, Burke, and Ernzerhof (PBE)[8] in generalized gradient approximation (GGA)[9] form were adopted to describe the exchange and correlation energy. The interaction between valence electrons (Ba $5s^2 5p^6 6s^2$, B $2s^2 2p^1$, O $2s^2 2p^4$ and F $2s^2 2p^5$) and atom cores was modeled by optimized norm-conserving pseudopotential[10], which allow us to adopt a relatively small plane-wave basis set without compromising the computational accuracy. The kinetic energy cutoff 900 eV and dense Monkhorst-Pack[11] k-point meshes spanning less than 0.05 $Å^{-1}$ in the Brillouin zone were chosen. Convergence test shows that these computational parameters are sufficiently accurate for this study.

It is well known that the band gaps are usually underestimated by GGA, due to the discontinuity of the exchange and correlation energy. In the optical properties calculations, the scissor operator[12] was adopted to shift all the calculated conduction bands to match the measured energy band gap. The imaginary part of the dielectric function was obtained from the electron transitions between the valence bands (VB) and conduction bands (CB), and then the real part of the dielectric function (and the refractive index n) can be calculated using the Kramers-Kronig transform[13]. To investigate the influence of the e^-_6 defect on the electronic and optical properties in $Ba_5(BO_3)_3F$, a simulation model was used in which a fluorine atom is directly removed in each unit cell. The O_1^- and O_5^- defect were not theoretically considered in this work due to the limitation of our first-principles method.

Acknowledgements

This work was supported by Russian Foundation for basic research (Grant 13-03-12158 ofi-m), the NSF of China (Grants 11174297 and 11474292), China "973" project (Grant 2011CB922204), and Special Foundation of the Director of Technical Institute of Physics and Chemistry, CAS.

Notes

[1]Institute of Geology and Mineralogy, SB RAS, 630090 Novosibirsk, Russia
[2]Beijing Center for Crystal R&D, Key Lab of Functional Crystals and Laser Technology of Chinese Academy of Sciences, Technical Institute of Physics and Chemistry, CAS, Beijing 100190, China
[3]University of Chinese Academy of Science, Beijing 100049, China
*Corresponding author, email: eliseev.ap@mail.ru , zslin@mail.ipc.ac.cn.

Reference.

1 T. B. Bekker, S. V. Rashchenko, V. V. Bakakin, Y. V. Seryotkin, P. P. Fedorov, A. E. Kokh and S. Y. Stonoga, *Crystengcomm*, 2012, 14, 6910-6915.
2 S. V. Rashchenko, T. B. Bekker, V. V. Bakakin, Y. V. Seryotkin, V. S. Sheychenko, A. E. Kokh and S. Y. Stonoga, *Cryst. Growth Des.*, 2012, 12, 2955-2960.
3 S. V. Rashchenko, T. B. Bekker, V. V. Bakakin, Y. V. Seryotkin, A. E. Kokh, P. Gille, A. I. Popov and P. P. Fedorov, *J. Appl. Crystallogr.*, 2013, 46, 1081-1084.
4 T. Alekel and D. A. Keszler, *Inorg. Chem.*, 1993, 32, 101-105.
5 A. Vegas, *Acta Crystallogr., Sect. C: Cryst. Struct. Commun.*, 1985, 41, 1689-1690.
6 S. J. Clark, M. D. Segall, C. J. Pickard, P. J. Hasnip, M. J. Probert, K. Refson and M. C. Payne, *Zeitschrift Fur Kristallographie*, 2005, 220, 567-570.
7 W. Kohn and L. J. Sham, *Phys. Rev.*, 1965, 140, 1133.
8 J. P. Perdew, K. Burke and M. Ernzerhof, *Phys. Rev. Lett.*, 1996, 77, 3865-3868.
9 J. P. Perdew, J. A. Chevary, S. H. Vosko, K. A. Jackson, M. R. Pederson, D. J. Singh and C. Fiolhais, *Phys. Rev. B*, 1992, 46, 6671-6687.
10 A. M. Rappe, K. M. Rabe, E. Kaxiras and J. D. Joannopoulos, *Phys. Rev. B*, 1990, 41, 1227-1230.
11 H. J. Monkhorst and J. D. Pack, *Phys. Rev. B*, 1976, 13, 5188-5192.

12 R. W. Godby, M. Schluter and L. J. Sham,Phys. Rev. *B*, 1988, 37, 10159-10175.
13 E.D. Palik, *Handbook of Optical Constants of Solids*, Academic Press,1985,190.
14 C. Furetta., *Handbook of thermoluminescense,* World Scientific, 2003,461
15 W.B. Fowler, *Physics of Color Centers,* Academic, 1968, chapters 2 and 4.
16 A. Abragam and M. H. L. Pryce, *Proc. R. Soc. London, Ser.* , 1951, 205, 135-153.
17 M. C. M. Obrien, *Proc. R. Soc. London, Ser.*, 1955, 231, 404-414.
18 O. F. Schirmer, *J. Phys. Chem. Solids.*, 1971, 32, 499.
19 B. Zhang, Z. Yang, Y. Yang, M.-H. Lee, S. Pan, Q. Jing and X. Su, *J. Mater. Chem. C*, 2014, 2, 4133-4141
20 H. Wu, H. Yu, Z. Yang, X. Hou, X. Su, S. Pan, K. R. Poeppelmeier and J. M. Rondinelli, *J. Am. Chem. Soc.*, 2013, 135, 4215-4218.
21 Z. Lin, X. Jiang, L. Kang, P. Gong, S. Luo and M.-H. Lee, *J. Phys. D: Appl. Phys.*, 2014, 47. 253001

Graphical Abstract

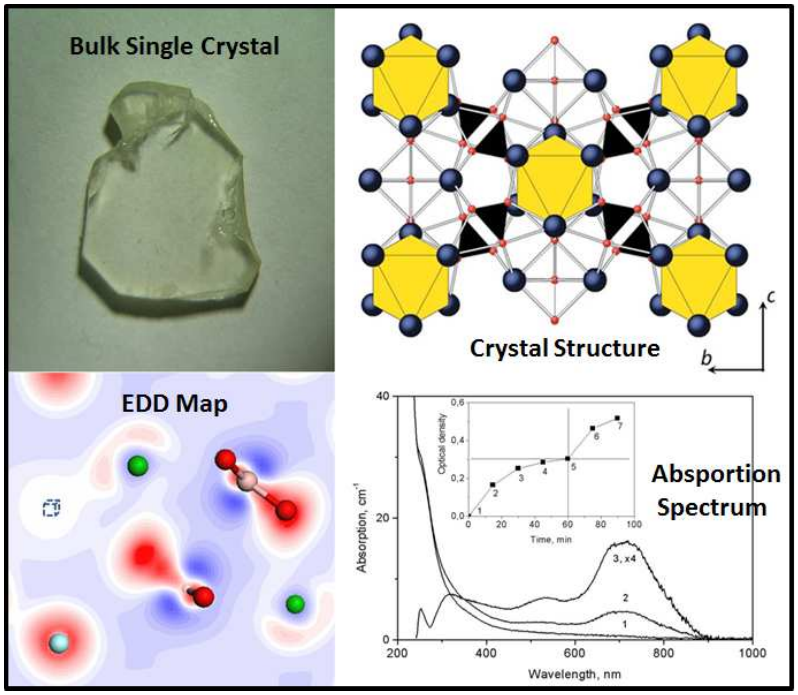

The optical properties of $Ba_5(BO_3)_3F$ in bulk single crystal are investigated experimentally and theoretically

Figure caption

Fig.1. Appearance (a) and PL pattern (b) of the polished plate of $Ba_5(BO_3)_3F$, 2 mm thick PL was excited by a 365 nm Hg light

Fig.2. Crystal structure of $Ba_5(BO_3)_3F$ in the representation of cation-coordinated anions, view along the *b*-axis(a) and the *a*-axis(b). F^- ions are in the centers of the yellow octahedra, black triangles represent $(BO_3)^{3-}$ anions, and Ba^{2+} cations are shown as dark-blue spheres[3]

Fig.3. (a) UV to near-IR and (b) mid-IR transmission for $Ba_5(BO_3)_3F$. Spectra 1 and 2 were recorded for 0.5 mm thick plate at 80 K and at 300 K, respectively. Curve 3 was measured for 2 mm thick plate at T=300 K. Spectra 4, 5, 6 show the transmission for BBO, LBO and CLBO plates 0.5 mm thick, in the IR region.

Fig.4. Absorption spectra for $Ba_5(BO_3)_3F$ before (1) and after X-irradiation (2).; Differential spectrum (3)=(2)-(1), was magnified 4 times for clarity. In the inset: Coloring kinetics at X-ray irradiation, recorded for 500 nm absorption in $Ba_5(BO_3)_3F$. Points 2-5 were recorded at irradiation through one face, the others were obtained after plate turn over, with irradiation through the opposite face.

Fig.5. Thermoluminescence curve in $Ba_5(BO_3)_3F$ after X-ray irradiation during 10 min.at 80 K.

Fig.6. PL spectra at 325 nm (1), 365 nm (2), 532 nm (3) excitations and RL spectrum (4), for $Ba_5(BO_3)_3F$. T= 300 K.

Fig.7. ESR spectrum for X-irradiated $Ba_5(BO_3)_3F$ crystal. T=80 K.

Fig.8. The scissor-corrected electron band structure near the band gap for perfect $Ba_5(BO_3)_3F$ (a) and for $Ba_5(BO_3)_3F$ with the e_6^- defect (b)

Fig. 9. The scissor-corrected electron energy total density of state and partial density of state of perfect $Ba_5(BO_3)_3F$ (a) and $Ba_5(BO_3)_3F$ with the e_6^- defect (b).

Fig. 10. The calculated dispersion curves for refractive indices n_x, n_y and n_z in $Ba_5(BO_3)_3F$.

Fig.11. The charge-density difference maps around the defects of e_6^-. The Ba, B, O and F atoms are represented by the green, pink, red and cyan balls, respectively, and the F vacancy is indicated by a dashed box. The color level goes from a reduction in density (blue) to a gain in density (red) and the units are e/A^2

Fig. 12. Calculated absorption spectra for the perfect $Ba_5(BO_3)_3F$ (1) and $Ba_5(BO_3)_3$ with the e_6^- defect (2).

Fig.1 Appearance (a) and PL pattern (b) of the polished plate of $Ba_5(BO_3)_3F$, 2 mm thick PL was excited by a 365 nm Hg light.

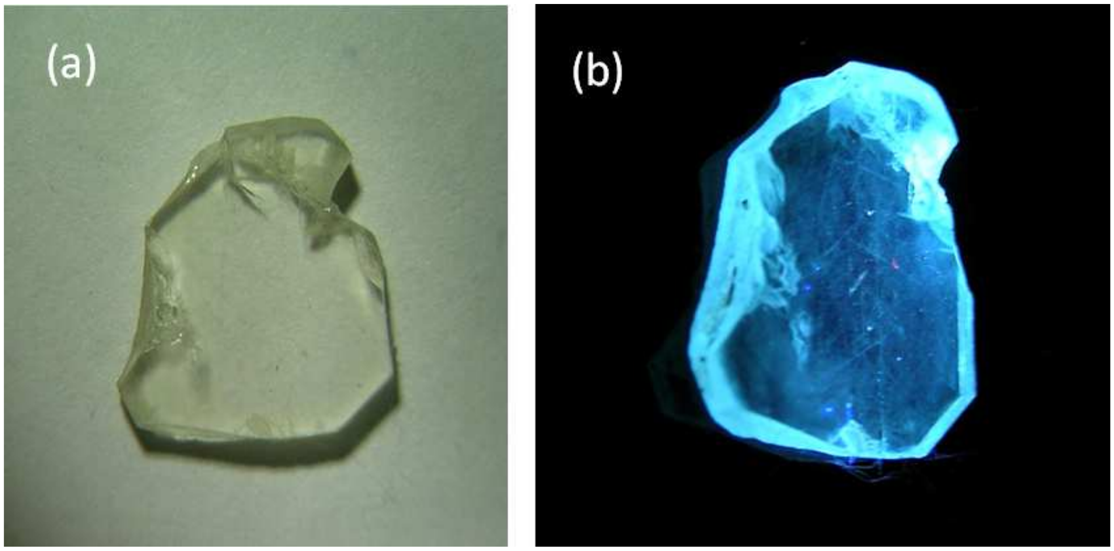

Fig.2. Crystal structure of $Ba_5(BO_3)_3F$ in the representation of cation-coordinated anions, view along the *b*-axis(a) and the *a*-axis(b). F^- ions are in the centers of the yellow octahedra, black triangles represent $(BO_3)^{3-}$ anions, and Ba^{2+} cations are shown as dark-blue spheres[3].

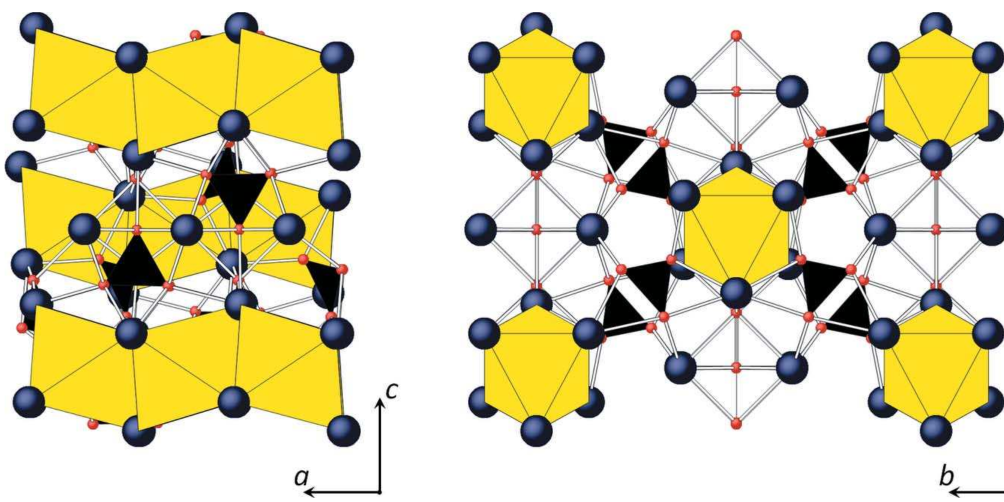

Fig.3. (a) UV to near-IR and (b) mid-IR transmission for $Ba_5(BO_3)_3F$. Spectra 1 and 2 were recorded for 0.5 mm thick plate at 80 K and at 300 K, respectively. Curve 3 was measured for 2 mm thick plate at T=300 K. Spectra 4, 5, 6 show the transmission for BBO, LBO and CLBO plates 0.5 mm thick, in the IR region.

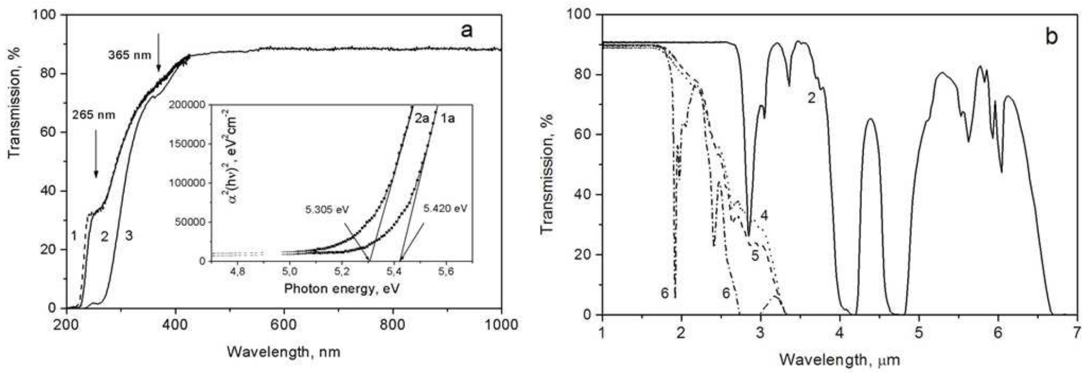

Fig.4. Absorption spectra for $Ba_5(BO_3)_3F$ before (1) and after X-irradiation (2).; Differential spectrum (3)=(2)-(1), was magnified 4 times for clarity. In the inset: Coloring kinetics at X-ray irradiation, recorded for 500 nm absorption in $Ba_5(BO_3)_3F$. Points 2-5 were recorded at irradiation through one face, the others were obtained after plate turn over, with irradiation through the opposite face.

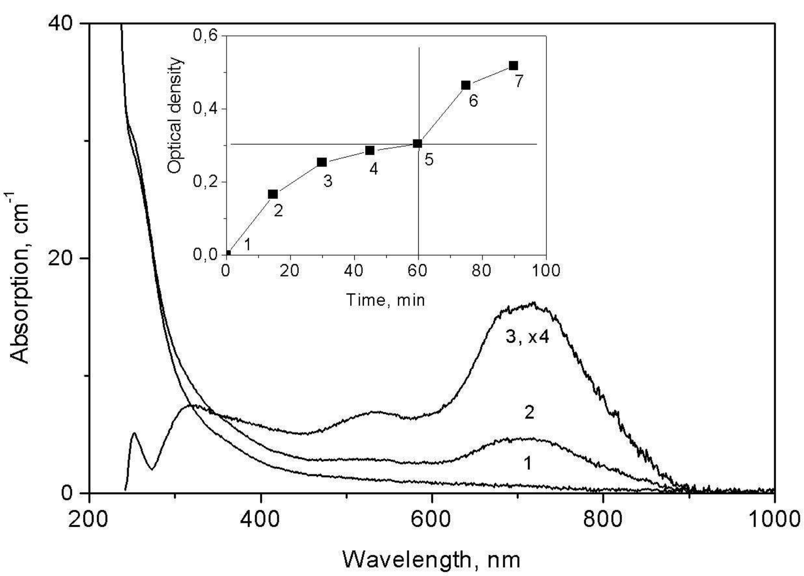

Fig.5. Thermoluminescence curve in $Ba_5(BO_3)_3F$ after X-ray irradiation during 10 min.at 80 K.

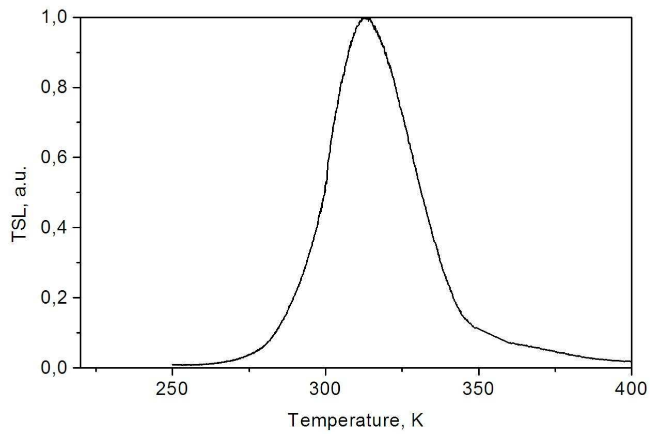

Fig.6. PL spectra at 325 nm (1), 365 nm (2), 532 nm (3) excitations and RL spectrum (4), for $Ba_5(BO_3)_3F$. T= 300 K.

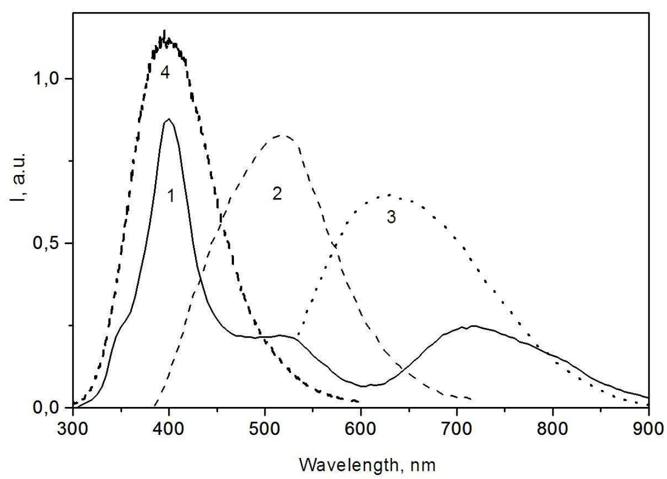

Fig.7. ESR spectrum for X-irradiated $Ba_5(BO_3)_3F$ crystal. T=80 K.

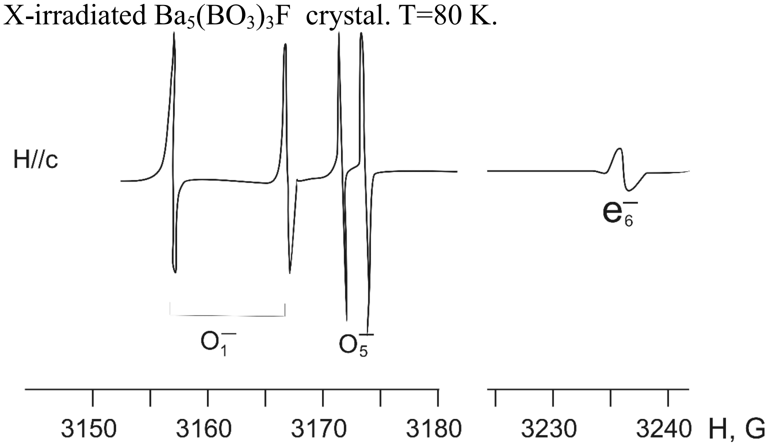

Fig.8. The scissor-corrected electron band structure near the band gap for perfect $Ba_5(BO_3)_3F$ (a) and for $Ba_5(BO_3)_3F$ with the e_6^- defect (b)

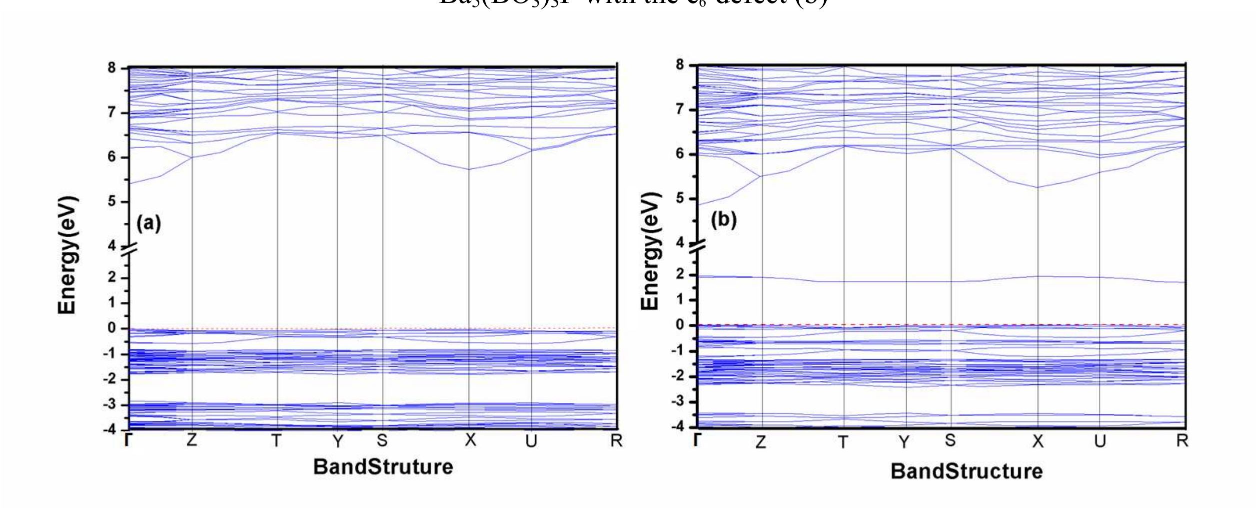

Fig. 9. The scissor-corrected electron energy total density of state and partial density of state of perfect $Ba_5(BO_3)_3F$ (a) and $Ba_5(BO_3)_3F$ with the e_6^- defect (b).

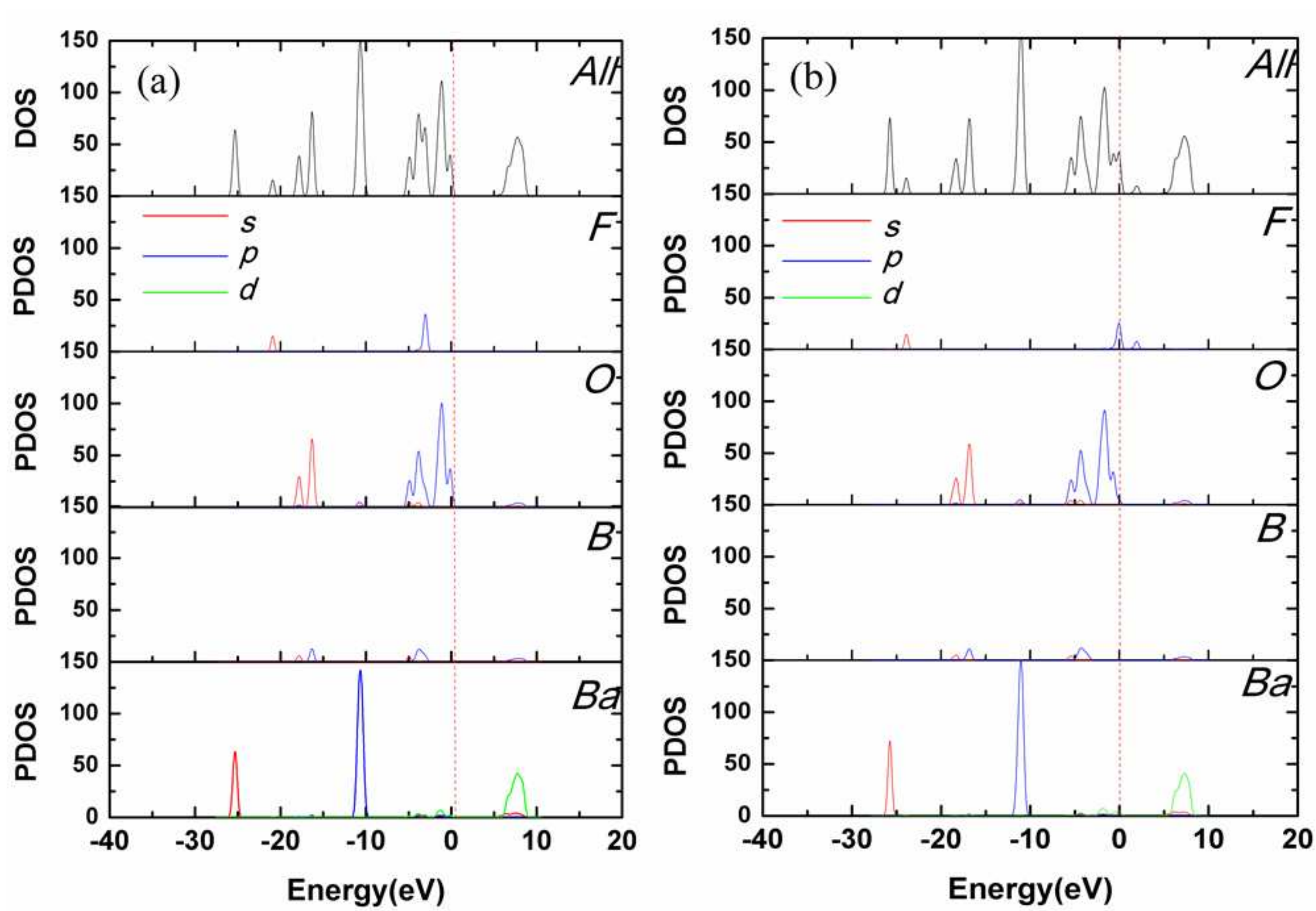

Fig. 10. The calculated dispersion curves for refractive indices n_x, n_y and n_z in $Ba_5(BO_3)_3F$.

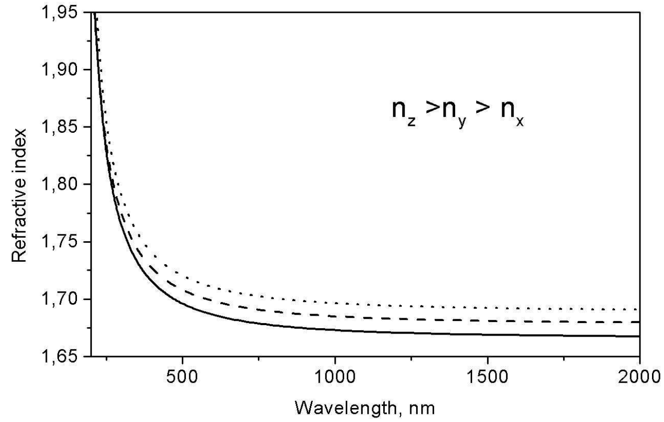

Fig.11. The charge-density difference maps around the defects of e_6^-. The Ba, B, O and F atoms are represented by the green, pink, red and cyan balls, respectively, and the F vacancy is indicated by a dashed box. The color level goes from a reduction in density (blue) to a gain in density (red) and the units are e/A^2

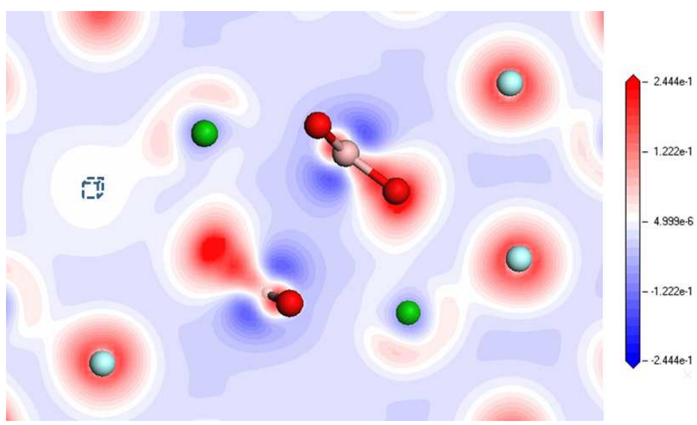

Fig. 12. Calculated absorption spectra for the perfect $Ba_5(BO_3)_3F$ (1) and $Ba_5(BO_3)_3$ with the e_6^- defect (2).